PCCP

PAPER

View Article Online
View Journal | View Issue

Cite this: *Phys. Chem. Chem. Phys.*, 2021, **23**, 10780

The O $K^{-2}V$ spectrum of CO: the influence of the second core-hole†

D. Koulentianos, ‡*[abc] S. Carniato,‡[a] R. Püttner, ‡[d] J. B. Martins,[a] O. Travnikova,[ae] T. Marchenko,[ae] L. Journel, [ae] R. Guillemin,[ae] I. Ismail,[ae] D. Céolin,[e] M. N. Piancastelli, [af] R. Feifel [b] and M. Simon [ae]

Received 8th February 2021,
Accepted 16th April 2021

DOI: 10.1039/d1cp00607j

rsc.li/pccp

Using synchrotron radiation in the tender X-ray regime, a photoelectron spectrum showing the formation of single site double-core-hole pre-edge states, involving the K shell of the O atom in CO, has been recorded by means of high-resolution electron spectroscopy. The experimentally observed structures have been simulated, interpreted and assigned, employing state-of-the-art *ab initio* quantum chemical calculations, on the basis of a theoretical model, accounting for their so-called direct or conjugate character. Features appearing above the double ionization threshold have been reproduced by taking into account the strong mixing between multi-excited and continuum states. The shift of the σ* resonance below the double ionization threshold, in combination with the non-negligible contributions of multi-excited configurations in the final states reached, gives rise to a series of avoided crossings between the different potential energy curves.

1 Introduction

Over the last decade, several experimental works reporting on the formation of double-core-hole (DCH) states in atoms and mainly in molecules, have been published.[1–22] DCH states are electronic states formed either by the ejection of two core electrons into the continuum (referred to as DCH continuum states), by a core-ionization core-excitation mechanism (referred to as DCH pre-edge states), or by a double core-excitation (referred to as neutrally excited DCH pre-edge states). A theoretical description of the former type of DCH states was initially given by Cederbaum *et al.*,[23] while the first experimental fingerprints of such states were identified in the work of Ågren *et al.*,[24] in the late seventies. Nevertheless, it was the development of third generation synchrotron radiation (SR) facilities[1–17] on one hand, and X-ray free electron lasers (XFEL)[18–22] on the other, which made the experimental observation of such states more easily accessible.

In what concerns molecular DCH continuum states, the creation of the two vacancies may occur either in the core shell of one atom (denoted as K^{-2}, for the case of K-shell vacancies), or in the core shells of two different atoms (denoted as $K^{-1}K^{-1}$ when different K shells are involved). The first case is referred to as single site (ss) DCH states, while the second as two site (ts) DCH states. As it was predicted in ref. 23, ts-DCH states will be characterized by enhanced chemical-shifts, allowing for a more sensitive probe of the chemical environment of an atom in a molecule, compared to the traditional electron spectroscopy for chemical analysis (ESCA) technique, developed by K. Siegbahn.[25] A theoretical investigation of this feature of ts-DCH states has been reported in ref. 26 for the formamide molecule and the nucleobases. On the other hand, ss-DCH states will be characterized by large orbital relaxation effects, as it was again theoretically predicted in ref. 23, and was further validated afterwords.[4,16]

Concerning the experimental observation of such states, upon single photon absorption using SR, the works of Eland *et al.*[1] and Lablanquie *et al.*[2] reported for the first time on the formation of ss-DCH continuum states in different small light-atom (C, N, O) containing molecules. In both ref. 1 and 2, the DCH continua were measured by means of time-of-flight (TOF) multi-electron coincidence spectroscopy, using a magnetic bottle spectrometer. With the same experimental setup, the ts-DCH continuum of the triply bonded C_2H_2 molecule was recorded shortly later,[3] and subsequently, Nakano *et al.*[5] measured the ss and ts-DCH continua of CO, N_2 and the C_2H_{2n}

[a] *Sorbonne Université, CNRS, Laboratoire de Chimie Physique-Matière et Rayonnement, F-75005 Paris Cedex 05, France*
[b] *Department of Physics, University of Gothenburg, Origovägen 6B, SE-412 96 Gothenburg, Sweden*
[c] *Chemical Sciences and Engineering Division, Argonne National Laboratory, 9700 S Cass Avenue, Lemont, IL 60439, USA. E-mail: koulentianos@anl.gov*
[d] *Fachbereich Physik, Freie Universität Berlin, Arnimallee 14, D-14195 Berlin, Germany*
[e] *Synchrotron SOLEIL, L'Orme des Merisiers, Saint-Aubin, BP 48, F-91192 Gif-surYvette Cedex, France*
[f] *Department of Physics and Astronomy, Uppsala University, Box 516, SE-751 20 Uppsala, Sweden*

† Electronic supplementary information (ESI) available. See DOI: 10.1039/d1cp00607j

‡ These authors contributed equally to this work.

(n = 1,2,3) series. Finally, this technique was used as well in order to perform DCH measurements in bigger molecules like propylene[6] (C_3H_6) and benzene[7] (C_6H_6). The limitations on the observation of the elusive ts-DCH states, using SR, have been demonstrated and discussed in ref. 6, for the case of ethyl trifluoroacetate ($C_4H_5F_3O_2$). Such limitations have been shown to be overcome, using instead of SR, the intense femtosecond pulses of an XFEL.[18–22]

Beyond DCH continuum states, the formation of a fully depleted K-shell through a simultaneous core-ionization core-excitation mechanism was observed in ref. 1, 8 and 10. Here, like in the case of DCH continuum states, a significant contraction of the valence orbitals takes place upon K-shell photoionization, which in turn leads to the shake-up of the second K-shell electron, instead of its shake-off like in the formation of a DCH continuum state. This type of DCH states is usually denoted as $K^{-2}V$, with V referring to the unoccupied valence or Rydberg orbital that the core-excited electron occupies. The interest for molecular states of such form stems from the fact that they access, in highly-symmetric molecules, final-state orbitals which are non-reachable through conventional near edge X-ray absorption fine structure (NEXAFS) spectroscopy. A detailed theoretical description of DCH pre-edge states has been given by Carniato *et al.*,[9] interpreting the observed spectral features in terms of their direct (dipolar ionization-monopolar excitation) and conjugate (monopolar ionization-dipolar excitation) nature, upon single photon absorption, similarly to the theoretical description of valence shake-ups initially given by Martin and Shirley.[27] In general, the $K^{-2}V$ signatures have been treated so far like NEXAFS features of the K^{-1} cation.

For the experimental observation of DCH pre-edge states, beyond TOF electron spectroscopy, high-resolution single electron spectroscopy, using a hemispherical electron analyser, has been proven to be a very efficient tool. The first experimental studies, using this technique, reported on the formation of $K^{-1}L^{-1}V$ states in argon[11] and $K^{-2}V$ in neon.[12] Concerning the observation of molecular $K^{-2}V$ states, Carniato and co-workers[13] recorded the core-ionized core-excited states involving the K shell of C atom in CO_2, while Feifel *et al.*[14] reported on the $K^{-2}V$ states of CS_2 and SF_6, involving the K shells of each and every atom. Both ref. 13 and 14, are two showcases for the advantages of $K^{-2}V$ spectroscopy, as for the centro-symmetric molecules studied there, the forbidden in NEXAFS spectroscopy g $\rightarrow$ g transitions were clearly observed. Accordingly, following the work done in ref. 11, the $K^{-1}L^{-1}V$ DCH states of the iso-electronic to argon HCl molecule[15] were investigated. Furthermore, a study of the $K^{-2}V$ states in CH_3CN, a molecule possessing two non-equivalent carbon atoms, along with a discussion of the factors contributing to the chemical-shift between them, can be found in ref. 16. Finally, a high-resolution electron spectrum, recording the $K^{-2}V$ states of water can be found in ref. 17. More recently, it was demonstrated from Mazza and coworkers,[28] for the case of Ne, how such $K^{-2}V$ resonances can be reached using instead of SR the light produced at an XFEL. XFEL studies are expected to shed light on the formation of DCH pre-edge states on third and higher row elements, which are characterized by very small cross-sections,[29] making their experimental observation using SR impracticable. Regarding the neutrally excited DCH states of the form $K^{-2}VV'$, where both core electrons have been excited to the V and V′ unoccupied molecular/Rydberg orbitals, though such states are known to be accessible through X-ray absorption spectroscopy (XAS),[30,31] yet no experimental evidence on their Auger decay is available to date. Finally, another interesting feature of DCH spectroscopy can be found in the probe of the induced nuclear dynamics, upon the formation of a double inner-shell vacancy. On one hand, the (sub)femto-second lifetimes of DCH states would not allow for a significant change of the molecular geometry, but on the other ''hand'', their highly repulsive potential energy surfaces, could even result in ultra-fast dissociation.[32,33]

Within the frame of the current work, the formation of $K^{-2}V$ DCH states, involving the K shell of O atom in CO has been recorded by means of single electron high-resolution spectroscopy. The experimental photoelectron spectrum has been reproduced by theoretical simulations, taking into account the direct and conjugate character of each observed transition, with experiment and theory being in very good agreement. Previously known aspects of $K^{-2}V$ spectroscopy, like the increased term values (TV) of the different pre-edge states and the shift of the σ^* transition below threshold, are present here. Nevertheless, as several avoided crossings appear in the potential energy curves (PEC) of the different final states, an interpretation of the observed spectral features as the K^{-1} analogue of the regular CO NEXAFS spectrum[34] should be treated with caution. A behaviour similar to the present $K^{-2}V$ spectrum has been observed in the $K^{-1}V$ absorption spectrum of O_2 molecule.[35–37] In the latter case, the below-threshold position of the σ^* resonance, within the Rydberg region, causes a series of avoided crossings, making the assignment of the different resonances non-trivial.

2 Experimental part

Experimental work was conducted at the French national synchrotron radiation facility SOLEIL, Saint Aubin, France. At the GALAXIES beamline[38] of SOLEIL, an experimental end-station fully dedicated to hard X-ray photoelectron spectroscopy (HAXPES)[39] is routinely available. The beamline operates in the tender to hard X-ray regime (2.3–13 keV). In brief, linearly polarized X-rays are delivered by a U20 undulator and are monochromatized by a Si(111) double crystal monochromator (DCM). Photoelectrons ejected from the sample, which is enclosed in a gas cell, are collected and analyzed with an EW4000 VG Scienta hemispherical analyzer, the electrostatic lens of which is parallel to the polarization vector of the incoming radiation and its acceptance angle can be either 45° or 60°. The resolution of the spectrometer is $\sim$1 eV at 500 eV pass energy and 800 mm slit size. The measurements for this work were performed using a photon energy of 2.3 keV. The photon energy bandwidth corresponding to this value is estimated to be 270 meV, *i.e.* it is only a small contribution to the total experimental resolution. Data acquisition took place over a 12 h time interval, with a constant pressure of 1.5×10^{-5} mbar at the chamber, while the pressure

in the gas cell is estimated to be two orders of magnitude higher than in the chamber. At the selected photon energy the photon flux of the beamline is at 1.5×10^{12} ph s^{-1}.

The energy calibration of the acquired spectra was performed in two steps. First the LMM Auger spectrum of argon was recorded, and the $L_3M_{2,3}M_{2,3}(^1S_0)$ transition at 201.09 eV[40] kinetic energy was used to calibrate the spectrometer. Subsequently, the photon energy was calibrated based on the binding energy of 248.63 eV for argon $2p_{3/2}{}^{-1}$.[41]

3 Theoretical details

In the present calculations, the $K^{-2}V$ process can be considered as a super shake-up phenomenon of single core-ionization, where the shaken electron is a K-shell electron. The direct and conjugate quantum paths, possible in this process, have been described here by a product of an one-electron matrix element times a $(N-1)$ term, which describes all other electrons in the molecule. For the direct path, a dipolar one-electron matrix element is associated with the overlap matrix integral between the $(N-1)$ initial and $(N-1)$ final state wave-functions. For the conjugate path, the one-electron overlap integral between the 1s inner-shell atomic orbital and the ejected photoelectron wave-function is associated with the remaining atomic dipole transition matrix integral between the $(N-1)$ initial and $(N-1)$ final wave-functions. The theory and related formulae are detailed in ref. 9.

The initial and final states have been described with a post Hartree–Fock (HF) configuration interaction (CI) procedure, using for oxygen an aug-cc-PCV5Z basis set[42] augmented by additional diffuse (s,p,d) orbitals, in order to better take into account Rydberg states and the relaxation of the valence orbitals in the presence of double core vacancies. A lighter cc-pVTZ basis set[42] was used for the neighboring carbon atom.

Our approach relies on the same set of orthogonal molecular orbitals (MO) for both the ground state of the neutral molecule, and the DCH states of the singly-ionized molecular ions. We made the choice to consider a set consisting of HF MOs optimized for the DCH K^{-2} ion. The final-state CI wave functions of the molecular ions are expanded over DCH (2h-1e) configurations, DCH/valence-hole (3h-2e) configurations and DCH/double-valence-hole (4h-3e) configurations.

The initial ground state has also been described at a CI level of theory including the main K^2 closed-shell configuration, $1\sigma^2(O_{1s})2\sigma^2(C_{1s})3\sigma^24\sigma^21\pi^45\sigma^2$, as well as the single core-hole, single core-hole and single valence-hole and double valence-hole excited configurations. In principle, in the HF Hamiltonian of an N-particle system, single-core excitations will not contribute because of the Brillouin theorem.[43] However, here the initial neutral ground state is built from the same set of the doubly core-ionized K^{-2} MOs as for $K^{-2}V$, *i.e.* quite far from the expected MOs corresponding to the neutral atom. Under these peculiar conditions, single-core and single core-valence excitations in the CI expansion of the initial state give tiny contributions, but are essential for the description of the direct process of the basic $K^{-2}V$ and $K^{-2}Vv' \rightarrow v''$ multi-excited states, (see previous works on this subject[8–10,14]). The large expansion used in this description allows compensating the relaxation effects induced by the DCH in the reference set. The choice of a unique reference set of molecular orbitals has also the advantage of providing a simple identification of contributing terms in, respectively, direct and conjugate cross sections. First, this unique set gives the dichotomous (0,1) values for the overall integrals taking part in the direct amplitudes. Second, it reduces the $(N-1)$-electron dipolar matrix elements taking part in the conjugate amplitudes, to single-electron matrix elements. The latter confirms that the CI expansions of the initial and final states are well balanced. All the configurations present in the description of the final state can be reached both through the direct and the conjugate paths, except for the (4h-3e) ones that would need the presence of (3h-3e) configurations in the ground state to be reached through the direct process.

While the peaks below the double ionization potential (DIP) can be essentially described as an ejection of one core electron accompanied by a single discrete transition, the situation is less straightforward in the region above the DIP, where one can expect the effect of coupling between the discrete multi-excited states and the double-ionization continuum. The simulation of this region taking into account the coupling effect is out of reach due to a huge number of CI configurations, but in order to adequately reproduce this region we adopted the following strategy.

In order to calculate the continuum profile of the spectrum a static-exchange (STEX-HF) approximation technique[44–49] has been adapted and combined with the Stieltjes imaging technique.[50,51] Our analysis reveals three main families of the CI states contributing to the spectrum above the DIP. In the first case, more than 90% of a CI state consists of a single (2h-1e) configuration. Since the corresponding core-excitation in the presence of a core-hole involves a vacant orbital located above the DIP, this state was considered as a pure continuum state. In the second case, more than 90% of a CI state consists of (3h-2e) and (4h-3e) configurations corresponding to discrete multi-excitations where core-excitations involve vacant orbitals located below the DIP. In this situation, similarly to the one encountered for the region below the DIP, the CI state was treated as a pure discrete state. In the third case, a CI state exhibits strong mixing between a single "continuum" state and various discrete "multiple-excitations" states. Therefore, for the sake of simplicity, these states and their associated cross sections were considered in the pool of the continuum states. The contribution of the discrete multi-excitations is superimposed to the simulated double continuum. Here we have assumed that there is no coupling/interference between the discrete and the double continuum parts.

Apart from this consideration, there is also a certain imbalance in the description of these core/valence excited electronic states compared to the final states in the region below the DIP. Indeed, if a correlation treatment at a CI level of theory, including single and double excitations CI(SD), is acceptable to treat formally $K^{-2}V$ single inner-shell excitations like in DCH (2h-1e) final states, namely the case for most of the peaks under the DIP, a larger

degree of correlation up to CI(SDTQ), *i.e.* taking into account also triple and quadruple excitations, is in principle required to be taken into account for the description of $K^{-2}Vv' \rightarrow v''$ states in the region above the DIP. This imbalance leads to calculated transition energies which are potentially too large. However, the calculation of electronic transitions becomes computationally very demanding with the inclusion of quadruple excitations leading to a very large configuration space, not possible to be treated with our home code. Thus, we can consider that the calculated $K^{-2}Vv' \rightarrow v''$ photoelectron satellites have too large energies (by 1 eV to 2 eV) compared to the experimental data. For better comparison between experimental and theoretical results, we have shifted the calculated $K^{-2}Vv' \rightarrow v''$ structures by 1 eV.

In the simulations, we make an assumption that the angular distribution parameter β associated with the direct shake-up is equal to 2 (p-wave) for the O 1s photoelectron, and equal to 0 for the conjugate shake-up (s-wave). Considering a half acceptance angle of $20^\circ \pm 10^\circ$ for the entrance lens of the analyzer, a factor of 2.8 ± 0.2 between the direct and the conjugate shake-up pathways is taken into account.[12]

The potential curve of the $^1\Sigma^+$ ground state of neutral CO was simulated with a Morse potential:

$$V(r) = D\cdot\left(1 - e^{-\rho(r-r_0)}\right)^2 \quad (1)$$

where the experimental dissociation energy D (0.4096 a.u.), fundamental frequency ω_e (2169 cm^{-1}), equilibrium internuclear distance (r_0 = 2.132 bohr) and anharmonicity constant ($\omega_e\chi_e \approx$ 15 cm^{-1}) were considered as parameters.[52] Within such conditions, ρ was fixed to 1.235 $bohr^{-1}$. For the vibrational motion, the eighteen first low-lying $^2\Sigma^+$ and $^2\Pi$ potential energy curves were calculated at the CI(SD) level of theory including single and double excitations with the GAMESS(US) package.[53] Some single energy points and corresponding numerical gradients along the stretching mode were also calculated at a DFT level of theory, using the Becke three-parameter hybrid exchange and the Lee–Yang–Parr (B3LYP) gradient-corrected correlation functional.[54,55]

In order to analyze the nature and properties of the most important transitions in the O $K^{-2}V$ spectrum of CO, a series of single point energy calculations at the DFT level of theory have been performed. In these calculations only one configuration within each state has been considered, namely the one with the highest coefficient, while all the other configurations have been neglected. Single point of energy with mono-determinantal technique must be taken with caution when strong interaction of few configurations occurs. However, this approach is useful to analyze various properties associated with each main configuration interacting at play. For that we have estimated a few different parameters, including (i) the mean value of the square root of the squared radius of the molecular orbital, (ii) the gradient (in eV $Å^{-1}$) at the initial equilibrium distance (1.128 Å); (iii) the width of the Franck–Condon envelope and (iv) the effective quantum number n^* deduced from the hydrogen-like formula $\sqrt{\langle r^2\rangle} = \alpha_0\sqrt{\frac{n^{*2}}{2Z^{*2}}(5n^{*2} + 1 - 3\ell(\ell+1))}$, ($\alpha_0$ being the bohr radius and ℓ = 0,1 for s and p states) and the corresponding term values compared to *ab initio* DFT/BL3LYP values.

4 Results and discussion

The assignment of the recorded structures is based on the results of the *ab initio* calculations described above. Our experimental spectrum, along with our theoretical simulations can be seen in Fig. 1. Visible are single shake-up final states of the form $K^{-2}V$ and the double shake-up final states of the form $K^{-2}Vv' \rightarrow v''$. As we will discuss in more detail further below, a number of avoided crossings can be seen in Fig. 2, which displays the different PECs. Because of this, in the CI calculations a number of states posses significant contributions of different configurations. To account for this finding, the different cationic $K^{-2}V$ states are labeled $n(^2\Sigma^+)$ and $n(^2\Pi)$. Here n is a counting index that increases with energy while Σ^+ and Π represent the symmetry of the state. More details on the configurations contributing to a certain state are given below and in Table S1 of the ESI.† Furthermore, from symmetry arguments it is straightforward that direct transitions will result in final states with Σ^+ symmetry while conjugate transitions are expected to lead to final states with both, Σ^+ and Π symmetries. Let us now discuss in more detail regions I–VI, as shown in Fig. 1.

4.1 Region I

Starting from region I in Fig. 1, a well isolated peak at ≈1156 eV binding energy in the experimental spectrum can be seen, corresponding to a transition to the $1(^2\Pi)$ state, having a pure conjugate (Π) character. From our *ab initio* calculations, the main results of which are summarized in Table S1 of the ESI,† it was found that the $K^{-2}2\pi^*$ configuration represents ≈92% of the CI state. This configuration is an excitation to the lowest unoccupied molecular orbital (LUMO) $2\pi^*$, the nodal structure of which (see Fig. S1 in the ESI†) shows an anti-bonding π^* MO, which has a dominant C 2p contribution in a linear combination of atomic orbitals (LCAO) scheme (see Tables S2 and S3, ESI†). Because of this high percentage and the excitation into the anti-bonding π^* orbital, we call the $1(^2\Pi)$ state also $K^{-2}2\pi^*$. Note that the calculated coefficients for the expansion of the states are given for the ground state equilibrium distance unless otherwise stated; they can significantly change with the internuclear distance, in particular when avoided crossings are involved, see below.

For the $2\pi^*$ orbital, the quantity $\sqrt{\langle r^2\rangle}$ was calculated at 1.44 Å at the HF level of theory and 1.41 Å at the DFT/B3LYP level of theory (see Tables S2 and S3 in the ESI†), thus close to that of the highest occupied molecular orbital (HOMO) 5σ (1.61 Å), indicating in this way a valence rather than a Rydberg character. The theoretical position of this transition was calculated at the DFT/B3LYP level of theory at 1153.8 eV, a value differing from the experimental value by 2.2 eV. It should be noted that such mismatches are systematic within a DFT treatment of DCH processes.[5–7] For that reason, the theoretical spectrum

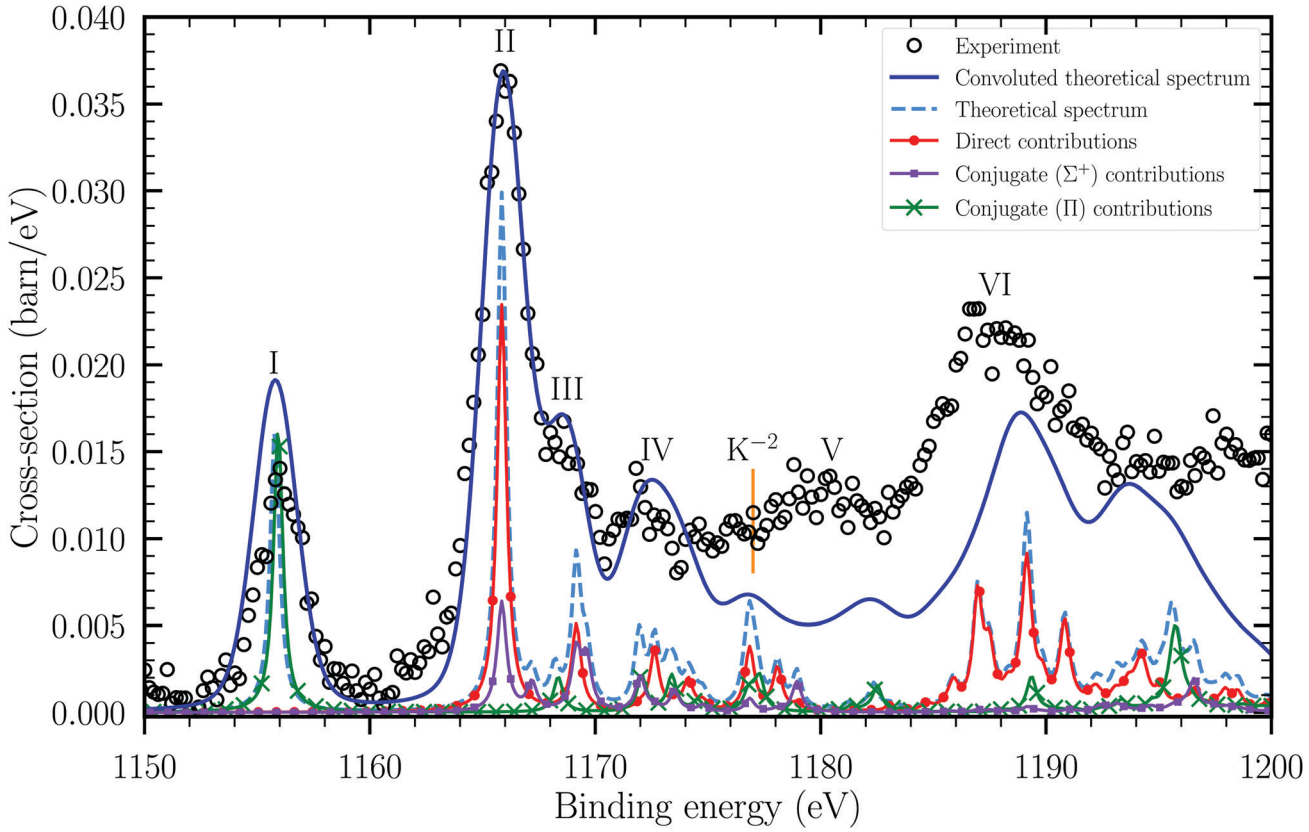

Fig. 1 An experimental photoelectron spectrum (black circles), recorded at a photon energy $h\nu$ = 2300 eV, showing the formation of several $K^{-2}V$ states, involving the O K edge of CO. The red circle-marked line shows the transitions taking place through the direct path, while the green x-marked line corresponds to the conjugate channel resulting in final states having an overall Π symmetry. The square-marked purple line shows final states reached through the conjugate channel having an overall Σ^+ symmetry. The dashed light blue line is the sum of the direct and conjugate sub-spectra. The different sub-spectra have been calculated at the CI level of theory. The dark blue solid line is the result of the sum of the different theoretical sub-spectra convoluted with our experimental resolution and a Gaussian profile, having a FWHM ≈ 2 eV, due to dissociative broadening. Finally, the orange vertical bar indicates the theoretical position of the K^{-2} threshold, obtained at the DFT/B3LYP level of theory, and shifted by 2.2 eV towards higher binding energy.

was blue-shifted to 1156 eV, in order to match the experimental excitation energy to the $1(^2\Pi)$ state.

The same shift has been applied to the value of the K^{-2} threshold (indicated with an orange bar in Fig. 1), resulting in a value of 1177 eV binding energy, in fairly good agreement with the experimental value of 1178.0 ± 0.8 eV, measured by Lablanquie *et al.*[2] From the aforementioned numbers, a TV of ≈22 eV is estimated for the transition to the 2π* MO, a value which is ≈2.5 times higher than the 8.97 eV estimated for the singly core-excited $K^{-1}2\pi^*$ state in ref. 34, where the vibrational sub-structure of the transition was also recorded, by means of photo-absorption spectroscopy. With the latter value being in excellent agreement with the TV of of 9.0 eV estimated in Sham *et al.*[56] by means of NEXAFS spectroscopy, and with the one of 8.3 eV obtained by Hitchcock and Brion[57] through electron energy loss spectroscopy (EELS), it is evident that the fully depleted K shell causes a strong attractive field, which shifts these core-ionized core-excited states away from threshold, as has been already found in several previous works focusing on the observation of $K^{-2}V$ states.[13,14,16]

A final point to be discussed, before moving on to region II, is the slope of the PEC of the $K^{-2}2\pi^*$ state, shown as a circle-marked light blue line in the middle panel of Fig. 2. As it was mentioned above, the PEC is strongly dissociative, which is also expected from the $Z + 2$ approximation as well. More specifically, it is known that the $K^{-2}\pi^*$ DCH state, for the iso-electronic case of N_2 is stable[10] and its equivalent $Z + 2$ approximation, NF^+ in the ground state, is also known to be stable.[58] In contrast, the equivalent of O $K^{-2}2\pi^*$ in CO is given by the noble-gas containing cation CNe^+, which is expected to be dissociative in the Franck–Condon region of CO in the ground state. As can be seen from Fig. 2, the extent of the Franck–Condon region is from ≈1.08 Å to ≈1.18 Å. We note that Frenking *et al.*[59] calculated the ground state of CNe^+ to be weakly bound with a dissociation energy D_e ≈ 130 meV and a bond length of 2.077 Å.

According to the Condon reflection approximation,[60] the slope of the PEC will depend on the full width at half maximum (FWHM) of the Gaussian profile describing the line-shape of the recorded transition, through $S = a\sigma$, as has been demonstrated in ref. 61, where S is the slope of the potential energy curve, σ the FWHM of the Gaussian and $a^2 = \mu\omega/\hbar$, with μ being the reduced mass of the molecule and ω its vibrational frequency in the electronic ground state. The line-shape of the transition will formally be described by a Voigt profile, being the result of

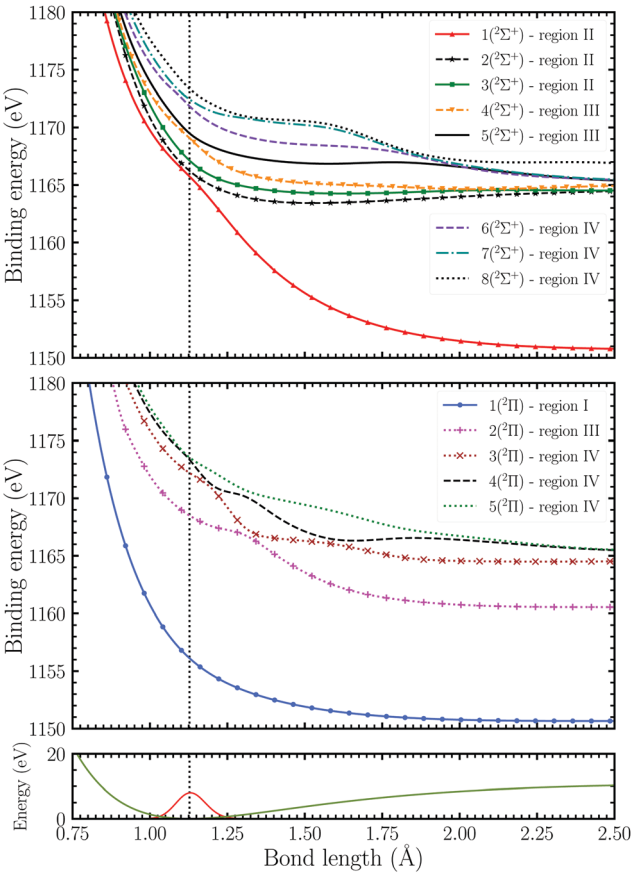

Fig. 2 Lower panel: The PEC (green line) of the electronic ground state ($^1\Sigma^+$) of CO, along with the Gaussian shaped ground state vibrational wavefunction, considering a Morse potential. Middle panel: Dissociative PECs of the different states reached through the conjugate channel, having a Π symmetry, observed below the K^{-2} double ionization threshold. Upper panel: PECs of the different states reached either through the direct channel or through the conjugate channel, having an overall Σ^+ symmetry, and observed below threshold.

the convolution of a Lorentzian profile accounting for the lifetime broadening, with a Gaussian profile having two contributions. The first is due to the experimental resolution, while the second is the result of the dissociative broadening. Yet, as it is explained below by giving the relative widths of each contribution, a Gaussian profile can adequately describe the above mentioned resonance, thus the value of the slope can be estimated from the width of the peak. From a fit analysis using a Gaussian profile, we obtained a value of σ = 1.90 ± 0.15 eV. Beyond the dissociative broadening, a Lorentzian profile of Γ_{DCH} = 513 meV, should also be used. The value of Γ_{DCH} above has been set equal to 3 × Γ_{SCH},[12,62] with Γ_{SCH} the lifetime of the O K^{-1} SCH state of CO taken from ref. 63. Finally, convolution with a Gaussian having a FWHM of 1 eV should be included, in order to properly account for the experimental resolution. From the values of the FWHM of the above mentioned profiles, it can be seen that the Gaussian part has a major contribution in the line-shape of the peak corresponding to the $K^{-2}2\pi^*$ state, therefore it was chosen for our fit analysis, instead of the more complex Voigt function. From the obtained value of σ, the value of the slope is estimated at −39.9 ± 3.2 eV Å^{-1}. This value is in relatively good agreement with the theoretical value of −33.2 eV Å^{-1} obtained at the DFT/B3LYP level of theory (Table S3 in the ESI†), yet it is significantly different from the CI numerical gradient of −24.9 eV Å^{-1}. The reason for the latter mismatch can be found in correlation effects, which are not treated properly within the CI method framework.

4.2 Region II

Continuing to region II, an intense spectral feature located at ≈1166 eV binding energy in the experimental spectrum is clearly visible in Fig. 1. This peak has been reproduced by our theoretical simulations, revealing that it predominantly consists of two transitions, the first and most intense one to the $1(^2\Sigma^+)$ state at 1165.80 eV binding energy, followed by a faint one to the $3(^2\Sigma^+)$ state at 1167.14 eV binding energy. At 1166.17 eV, *i.e.* between these two transitions contributing to the spectra, the $2(^2\Sigma^+)$ state is expected to be present. It consists of ≈92% of the $K^{-2}5\sigma^1 2\pi^{*2}$ as well as $K^{-2}5\sigma^1 2\pi'^{*2}$ configurations and has, therefore, practically no intensity (the notations π,π′ are explained in Table S1, ESI†). However, these configurations are strongly dissociative and lead to a number of avoided crossings as will be discussed in the following.

For the first peak at 1165.80 eV, the $K^{-2}6\sigma$ configuration was found from our theoretical investigations to be ≈77% of the CI state, at the equilibrium distance of the electronic ground state (see Table S1, ESI†), with the final state MO having a strong oxygen 3s character, with a less intense, yet non-negligible, carbon 3p (lying along the inter-nuclear axis) contribution (see Fig. S2 and Tables S2 and S3 of the ESI†). As shown in Fig. 1, this structure has a dominant direct component, though its conjugate (Σ^+) character is not negligible. In addition, from our theoretical results it was found that a strong mixing with the $K^{-2}7\sigma^*$ and the $K^{-2}5\sigma^1 2\pi^{*2}$ configurations takes place. The 7σ* orbital of the former configuration shows a nodal structure typical for the unoccupied σ* orbital obtained in the LCAO approach from the 2pσ orbitals of carbon and oxygen. In the latter configuration an electron from the 5σ MO has been promoted to the 2π*, being now doubly occupied. We note that the latter configuration is allowed under the ΔΛ = 0, ±1 selection rule.

For the 6σ orbital, the $\sqrt{\langle r^2\rangle}$ was estimated at 1.85 Å at the DFT/B3LYP level of theory (Table S3, ESI†), concomitant with a quantum defect of δ = 0.8, or equivalently a small effective quantum number n^* = n − δ = 2.2. The values of $\sqrt{\langle r^2\rangle}$ and n^*, in the HF level of theory, are predicted at 2.07 Å and 2.20, respectively (Table S2, ESI†). Note that the size of the 6σ orbital is comparable to the size of the valence orbitals 2π* and 7σ*, although from its nodal structure it has a strong O 3s and C 3p character (see Fig. S2, ESI†). Obviously, the high positive charge due to the DCH, seen by this orbital, causes a significant contraction. As a result, it does not experience the molecular dication as almost point-like and cannot be considered a pure Rydberg orbital, but has to be considered as an orbital with significant valence character, *i.e.* it has an influence on the

molecular bond. Despite its size, the shape of the 6σ orbital can be considered mainly as 3s-like (see Fig. S2 in the ESI†). In the SCH studies of ref. 34, 56 and 57, a similar $K^{-1}3s\sigma$ transition to a Rydberg orbital was identified, with its TV estimated at ≈3.6 eV in ref. 34 and 56. From the recorded peak position and the calculated K^{-2} threshold, the TV of the $1(^2\Sigma^+)$ state is estimated at ≈11 eV, thus increased by a factor of 3 compared to the SCH case, for the same reasons as explained above.

The PEC of the $1(^2\Sigma^+)$ state is shown with triangle-marked red solid line in the upper panel of Fig. 2. At the internuclear distance of ≈1.2 Å the slope becomes steeper due to an avoided crossing with the $2(^2\Sigma^+)$ state (star-marked dashed black line). The energetic limit at large internuclear distances is identical to that of the $K^{-2}2\pi^*$ state, because the same atomic states are involved. Thus we can conclude that at larger bond distances the $K^{-2}7\sigma^*$ configuration, including the anti-bonding σ* orbital, becomes dominant.

The CI gradient at the equilibrium distance associated to the $1(^2\Sigma^+)$ state was found at −27.2 eV $Å^{-1}$, and the deduced CI Franck–Condon FWHM at 1.5 eV. Additionally, if the O K^{-2} core-hole lifetime and the experimental resolution are taken into account, this value becomes 2.15 eV, which is in reasonable agreement with the experimental value of ≈2.5 eV. Considering on the other hand a single-point energy for the $K^{-2}6\sigma$ configuration, the DFT gradient was estimated at −40.0 eV $Å^{-1}$ (Table S3 in the ESI†), with the deduced numerical FWHM of the corresponding Franck–Condon envelope at 2.25 eV. However, it should be pointed out here that there are two possible explanations for the differences between experiment and theory. First, the Franck–Condon approximation is not strictly valid due to the avoided crossing at the upper limit of the Franck–Condon region. Second, contributions of transitions to the $3(^2\Sigma^+)$ state also show up at higher binding energies of the peak in region II.

The PEC shown by the star-marked black dashed line corresponds to a $2(^2\Sigma^+)$ state, which mainly consists of the configurations $K^{-2}5\sigma^12\pi^{*2}$ as well as $K^{-2}5\sigma^12\pi'^{*2}$ at the equilibrium distance of the ground state, *i.e.* it is reached after a K → 2π* transition accompanied by an additional 5σ → 2π* excitation. Within the framework of our model, the intensity of this line contributes only through the direct path from the initial O $K^15\sigma^12\pi^{*2}$ configuration of the ground state, which leads to $K^{-2}5\sigma^12\pi^{*2}$ configuration after photon absorption and K-shell ionization. However, such core-valence excited configurations play a minor role in the neutral ground state and the final cross-section is very weak. We note here that the $K^{-2}5\sigma^12\pi^{*2}$ state can be formed as well through the doubly core-excited $K^{-2}5\sigma^22\pi^{*2}$ configuration, which contributes to the ground state, after valence ionization of the 5σ MO. This valence ionization channel could interfere with the core-valence direct path described above, but has not been considered in the present study. The main relevance of the $K^{-2}5\sigma^12\pi^{*2}$ configuration for the present study is probably that it leads to avoided crossings.

The weak structure, theoretically predicted at 1167.14 eV, is caused by a transition to the $3(^2\Sigma^+)$ state. Its PEC is shown with the square-marked green solid line in Fig. 2. For this state the same configurations as for the $1(^2\Sigma^+)$ state should interact, but in addition, a $K^{-2}8\sigma$ configuration is also present there. Nonetheless, as the two lines caused by the transitions to the $1(^2\Sigma^+)$ and $3(^2\Sigma^+)$ state are very close in energy, they can not be resolved experimentally.

4.3 Region III

Moving forward, an intense shoulder on the right of the strongest spectral feature can be observed at ≈1168.5 eV binding energy (region III). As shown in Fig. 1 and Table S1 of the ESI,† this shoulder is caused by three different transitions, namely in energy order $2(^2\Pi)$, $4(^2\Sigma^+)$, and $5(^2\Sigma^+)$. More specifically, our theoretical results indicate that the strongest contributions are caused by the transition to the $4(^2\Sigma^+)$ state. The main contributions to this state are the single shake-up configurations $K^{-2}7\sigma^*$ (56%) and a double shake-up configuration $K^{-2}5\sigma^12\pi^{*2}$ (35%). Thus the transition has predominantly a valence character, which is in accordance with the value of $\sqrt{\langle r^2\rangle}$ at 2.40 Å, predicted again at the DFT/B3LYP level of theory. The PEC of the $4(^2\Sigma^+)$ state is shown with the invert triangle-marked dashed orange line in Fig. 2. It is the state which shows the strongest contribution of the $K^{-2}7\sigma^*$ configuration for which the excited state orbital is identified as the anti-bonding σ_{CO}^* MO (see above and Fig. S2 in the ESI†), recognized as the shape resonance[64,65] in SCH studies and observed well above threshold there. Because of that, the $4(^2\Sigma^+)$ is a highly dissociative state, with its PEC slope estimated at the DFT/B3LYP level of theory to be at −48.2 eV $Å^{-1}$ (Table S3 in the ESI†). Its TV in ref. 56 and 57 was estimated at ≈−9 eV, while here it is found at ≈8.5 eV, thus shifted by ≈17.5 eV. Such a pronounced shift of this specific structure is characteristic of the $K^{-2}V$ spectroscopy and has been observed in several related studies.[10,13,14,16] Finally, we note that in the same energy region, the states $2(^2\Pi)$, indicated by the pink dotted cross-marked PEC in Fig. 2, and $5(^2\Sigma^+)$, indicated by the black solid PEC, are present. The former state is predicted at 1168.4 eV and is dominated by the $K^{-2}3\pi$ configuration, while the latter state is predicted at 1169.6 eV and dominated by the $K^{-2}8\sigma$ configuration. The density plots of the excited-state orbitals 3π and 8σ can be seen in Fig. S1 and S2 (ESI†), respectively, and show a dominant O 3p character. An experimental observation of the $K^{-1}3p(\sigma,\pi)$ excitations has been reported in ref. 34, with its TV at ≈ 2.6 eV, reduced by a factor of 3 from its DCH counterpart, in line with the above mentioned observations.

As shown in the upper panel of Fig. 2, a second avoided crossing within the Franck–Condon region, is present between the $4(^2\Sigma^+)$ and the $5(^2\Sigma^+)$ PECs, while in the middle panel of Fig. 2, an avoided crossing in the edges of the Franck–Condon region between the $3(^2\Pi)$ and $4(^2\Pi)$ PECs is also evident. Because of their presence, the given assignments are valid only within the Franck–Condon region and a one-to-one correspondence with the NEXAFS study of the neutral species in ref. 34 should not be attempted. This can be explained by the below-threshold shift of the 7σ* resonance and states of the type $K^{-2}5\sigma^{-1}2\pi^*(^3\Pi)n\sigma(^2\Pi)$ which are both strongly dissociative. This results in the diabatic picture in a crossing with the K^{-2}Ryd states which are metastable with a potential-well depth of about 1 eV

and an equilibrium distance of ≈1.55 Å found when the present PECs are transfered to a diabatic picture. Similar values, namely a dissociation energy of 1.6 eV and an equilibrium distance of 1.67 Å have been found in calculations performed for the $Z + 2$ molecule CNe^{2+}, see ref. 66. In case of the K^{-1} resonant excitations, these states with a different bond character are well separated in energy. The significantly different behaviour of the cationic and neutral CO, found here, is in line with the results of a recent theoretical and experimental study by Couto and co-workers,[67] where the NEXAFS spectra, involving both the O and C K edges were recorded for CO^+, after the creation of an initial $5\sigma^{-1}$ vacancy.

4.4 Region IV

The last experimentally observed structure, before the K^{-2} threshold, has been recorded at ≈1172 eV binding energy and is labelled region IV in Fig. 1. Theoretically, this region is predicted to consist of several transitions having both direct, as well as conjugate (Σ^+,Π) character. More specifically, according to the results of our calculations, transitions to the final states $6(^2\Sigma^+)$ to $10(^2\Sigma^+)$ and $3(^2\Pi)$ to $5(^2\Pi)$ contribute to this region, with $6(^2\Sigma^+)$ and $7(^2\Sigma^+)$ being the most intense ones (see Table S1, ESI†). From the experimental spectrum, the TV of the peak is estimated at ≈5 eV. This value is in good agreement with the TVs obtained at the DFT level of theory of 5.62 eV for $K^{-2}9\sigma$, having a dominant O 4s character, and of 4.90 eV eV for $K^{-2}4\pi$. For the $n = 5$ Rydberg transitions, theory predicts TVs of 2.88 eV for $K^{-2}5\pi$ and 3.00 eV for $K^{-2}12\sigma$, the latter having a strong O 5s and 5p character. Interestingly, in the work of Püttner *et al.*,[34] the TVs of the $K^{-1}4p\pi$ and $K^{-1}5p\pi$ Rydberg transitions have been estimated at ≈1.26 eV and ≈0.72 eV, respectively. These values are smaller by a factor of 4 compared to the TVs estimated here, which reflects the Z^2 dependence of the Rydberg formula[15] in the presence of a fully depleted K shell, as is the case here.

Before we discuss the PECs of the states $6(^2\Sigma^+)$ to $8(^2\Sigma^+)$ and in particular $3(^2\Pi)$ to $5(^2\Pi)$, we want to point out that the state $K^{-2}5\sigma^{-1}1\pi^{-1}(^3\Pi)6\sigma$ has also been calculated at a binding energy of 1174.6 eV and could contribute to the peak IV at 1172 as a conjugate channel. This finding is in agreement with calculations for the dication CNe^{2+}, see ref. 66, which represents the $Z + 2$ approximation for the K^{-2} states of CO. In CNe^{2+} the states $\sigma^{-1}\pi^{*1}(^3\Pi)$, $\sigma^{-1}\pi^{*1}(^1\Pi)$, and $\sigma^{-1}\pi^{*1}(^3\Sigma)$ are 4.6 eV, 8.7 eV, and 10.8 eV, respectively, above the K^{-2} ground state. These values are in reasonable agreement with the splittings calculated for the double-shake states. Based on these considerations we can expect dissociative $K^{-2}5\sigma^{-1}1\pi^{-1}(^3\Pi)n\lambda$ states below the K^{-2} threshold, which have a significant influence on the PECs.

The dissociative PECs of the states $6(^2\Sigma^+)$ to $8(^2\Sigma^+)$ are shown in the upper panel of Fig. 2 with the dashed purple, dashed-dotted cyan and dotted black lines, respectively. The PECs of the $3(^2\Pi)$ to $5(^2\Pi)$ states are shown in the middle panel of Fig. 2, with the x-marked dotted brown, black dashed and dotted green lines, respectively. The strong interactions of the final states corresponding to the above mentioned configurations are reflected again in the avoided crossings between the different PECs. The most prominent level crossings are at ≈1.33 Å between the $2(^2\Pi)$ and $3(^2\Pi)$ states, and at ≈1.20 Å between the $3(^2\Pi)$ and $4(^2\Pi)$ states. By converting the adiabatic picture to a diabatic picture, *i.e.* by eliminating the avoided level crossings, one obtains a strongly dissociative state, which is described in the limit of long internuclear distances by the cross-marked pink dotted curve labeled $2(^2\Pi)$ and has at the equilibrium distance of the ground state an energy of ≈1168 eV. The latter value suggests in agreement with our calculations that the dissociative configuration is given by $K^{-2}5\sigma^{-1}1\pi^{-1}(^3\Pi)6\sigma$, see above. This configuration is expected to be dissociative and crosses the K^{-2}Ryd states, which are expected to be weakly bound in the diabatic picture, see above.

In the PECs a number of additional avoided level crossings can be observed, so for example at ≈1.60 Å between $3(^2\Pi)$ and $4(^2\Pi)$ as well as at ≈1.35 Å between $4(^2\Pi)$ and $5(^2\Pi)$ states. These avoided crossings are probably due to other dissociative $K^{-2}5\sigma^{-1}1\pi^{-1}(^3\Pi)n\lambda$ configurations. In particular, at the equilibrium distance of the ground state, a double shake-up $K^{-2}5\sigma^{-1}1\pi^{-1}(^3\Pi)7\sigma^{\star}$ state is theoretically predicted at ≈ 1177 eV binding energy. The corresponding peak can be seen in the calculations displayed in Fig. 1, together with two more peaks at ≅1178 and ≅1179 eV, which probably belong to transitions to the same kind of states.

The slight mismatch between the experimental and the theoretical intensities can be explained by the formation of a well known background, which has been observed in several $K^{-2}V$ studies.[11,15,16] This background is caused by the higher n unresolved Rydberg states below threshold, as well as the slow electron of the double ionization process above threshold, and can be modeled by an arctan function,[68] being the result of the convolution of a step function with the Lorentzian profile describing the lifetime broadening of the core-excited state.

4.5 Regions V & VI

The above threshold, higher binding energy regions of the spectrum, denoted as V and VI in Fig. 1, shall be discussed next. Starting from the former region, it can be seen from Fig. 1, that a low intensity broad spectral feature is visible at ≈1180 eV binding energy. This feature is well reproduced by our theoretical model, which predicts a low intensity conjugate (Π) transition at 1182.60 eV binding energy, having a double shake-up character. From our theoretical analysis it was found that the dominant configuration contributing to this state is $K^{-2}1\pi^1 2\pi^{*2}$, resulting in a doubly occupied LUMO. A high intensity peak is clearly visible in the experimental spectrum at ≈1187 eV binding energy (region VI). This structure consists of three different transitions having a dominant direct character, with their energy positions theoretically predicted at 1187.20 eV, 1189.03 eV and 1190.65 eV. These lines were found theoretically to be built by multi-shake-up configurations, involving the 1π MO, though this time, in addition to the LUMO, ns or np (n = 3,4,5) Rydberg states are occupied by the second excited electron. Theory also predicts that this intense above-threshold structure should be followed by a less pronounced peak at 1194 eV binding energy, being the result of several transitions having either a direct or a conjugate (Σ^+,Π) character. Yet, this structure is difficult to be identified

in our experimental spectrum. A final point to be noted here is that for the iso-electronic case of N_2 in ref. 10, no above threshold features were recorded so far.

5 Conclusions

We presented a combined experimental and theoretical study, discussing the DCH pre-edge states involving the K shell of the O atom in CO. The observed spectral features were well reproduced and assigned considering their direct or conjugate nature, while a remarkable agreement between experiment and theory for the above-threshold region, was achieved by superimposing multi-excited states into the double ionization continuum. Furthermore, PECs of the occupied final states below the K^{-2} threshold were calculated and a comparison of experimental with theoretical results was given for the value of the slope of the $K^{-2}2\pi^*$ LUMO-transition. The increased TVs of DCH states (by a factor of ≈ 3 compared to their SCH counterparts), associated with the formation of a fully depleted K shell were also observed in our study.

From a more general point of view we found that the O $K^{-2}V$ spectrum of CO is more complex than the O $K^{-1}V$ of the same molecule. In the latter spectrum the O 1s $\rightarrow$ $2\pi^*$ and the O 1s $\rightarrow$ Ryd resonances below the ionization threshold are well separated from the O 1s $\rightarrow$ σ^* shape resonance and the double excitations. This separation does not exist for the DCH states and leads to a number of avoided level crossings and consequently to significant mixing of different configurations. It can be explained by three findings. First, the unoccupied σ^* valence orbital, which is normally present above the ionization threshold in SCH studies and is known as shape resonance, is in the present study significantly below threshold. Second, in the present case the $K^{-2}v' \rightarrow v''$ satellites are energetically closer to the K^{-2} state than the $K^{-1}v' \rightarrow v''$ satellites to the K^{-1} threshold. Third, the term value of the excited state orbital V in the $K^{-2}Vv' \rightarrow v''$ double shake-up states is larger than in the $K^{-1}Vv' \rightarrow v''$ doubly exited states due to the higher charge seen by this orbital in the DCH states. Since the last argument is expected to hold in general and since the shift of the unoccupied σ^* valence orbital from above threshold in SCH states to below threshold in DCH states has been observed already for a number of molecules, we expect that the higher complexity of the $K^{-2}V$ spectra is a general phenomenon. This result suggests that an interpretation of $K^{-2}V$ structures as cationic K^{-1} absorption lines should be treated with caution, as the assignment of the different features might become non-trivial due to the avoided crossings, especially if a significant change in the equilibrium geometry takes place. This is not the case in the present work, as the equivalent bond length of the molecule in its electronic ground state is at 1.128 Å,[69] while the bond length of the O doubly core-ionized CO has been calculated at 1.160 Å.[70] However, further investigations on similar systems like N_2, NO, and O_2 are necessary to shed more light on the matter. Finally, multi-shake-up excitations involving the occupied MOs of the CO molecule have been observed and give rise to an intense above-threshold spectral feature.

Author contributions

D. K., R. P., M. N. P. and M. S. devised research. D. K., R. P., J. B. M., O. T., T. M., L. J., R. G., I. I., D. C., M. N. P. and M. S. participated in the experiment. D. K., S. C. and R. P. performed data analysis. S. C. performed theoretical simulations. D. K., S. C. and R. P. wrote the paper and all the authors discussed the results and commented on the manuscript.

Conflicts of interest

There are no conflicts to declare.

Acknowledgements

D. K. and R. F. acknowledge financial support by the Swedish Research Council (VR) and the Knut and Alice Wallenberg Foundation, Sweden. D. K. wishes to acknowledge financial support by LabEx MiChem, France. D. K. also acknowledges support from the U.S. Department of Energy, Office of Basic Energy Sciences, Division of Chemical Sciences, Geosciences and Biosciences through Argonne National Laboratory. Argonne is a U.S. Department of Energy laboratory managed by UChicago Argonne, LLC, under contract DE-AC02-06CH11357. The experiments were conducted at the GALAXIES beam line of the synchrotron radiation facility SOLEIL, France (project no. 9918102), and the authors are grateful to the staff of SOLEIL for the smooth operation of the facility.

Notes and references

1 J. H. Eland, M. Tashiro, P. Linusson, M. Ehara, K. Ueda and R. Feifel, *Phys. Rev. Lett.*, 2010, **105**, 213005.
2 P. Lablanquie, F. Penent, J. Palaudoux, L. Andric, P. Selles, S. Carniato, K. Bučar, M. Žitnik, M. Huttula and J. Eland, *et al.*, *Phys. Rev. Lett.*, 2011, **106**, 063003.
3 P. Lablanquie, T. Grozdanov, M. Žitnik, S. Carniato, P. Selles, L. Andric, J. Palaudoux, F. Penent, H. Iwayama and E. Shigemasa, *et al.*, *Phys. Rev. Lett.*, 2011, **107**, 193004.
4 P. Linusson, O. Takahashi, K. Ueda, J. Eland and R. Feifel, *Phys. Rev. A: At., Mol., Opt. Phys.*, 2011, **83**, 022506.
5 M. Nakano, F. Penent, M. Tashiro, T. Grozdanov, M. Žitnik, S. Carniato, P. Selles, L. Andric, P. Lablanquie and J. Palaudoux, *et al.*, *Phys. Rev. Lett.*, 2013, **110**, 163001.
6 F. Penent, M. Nakano, M. Tashiro, T. Grozdanov, M. Žitnik, K. Bučar, S. Carniato, P. Selles, L. Andric and P. Lablanquie, *et al.*, *J. Electron Spectrosc. Relat. Phenom.*, 2015, **204**, 303–312.
7 S. Carniato, P. Selles, A. Ferté, N. Berrah, A. Wuosmaa, M. Nakano, Y. Hikosaka, K. Ito, M. Žitnik and K. Bučar, *et al.*, *J. Chem. Phys.*, 2019, **151**, 214303.
8 M. Nakano, P. Selles, P. Lablanquie, Y. Hikosaka, F. Penent, E. Shigemasa, K. Ito and S. Carniato, *Phys. Rev. Lett.*, 2013, **111**, 123001.
9 S. Carniato, P. Selles, L. Andric, J. Palaudoux, F. Penent, M. Žitnik, K. Bučar, M. Nakano, Y. Hikosaka and K. Ito, *et al.*, *J. Chem. Phys.*, 2015, **142**, 014307.

10 S. Carniato, P. Selles, L. Andric, J. Palaudoux, F. Penent, M. Žitnik, K. Bučar, M. Nakano, Y. Hikosaka and K. Ito, *et al.*, *J. Chem. Phys.*, 2015, **142**, 014308.
11 R. Püttner, G. Goldsztejn, D. Céolin, J.-P. Rueff, T. Moreno, R. K. Kushawaha, T. Marchenko, R. Guillemin, L. Journel and D. W. Lindle, *et al.*, *Phys. Rev. Lett.*, 2015, **114**, 093001.
12 G. Goldsztejn, T. Marchenko, R. Püttner, L. Journel, R. Guillemin, S. Carniato, P. Selles, O. Travnikova, D. Céolin and A. Lago, *et al.*, *Phys. Rev. Lett.*, 2016, **117**, 133001.
13 S. Carniato, P. Selles, P. Lablanquie, J. Palaudoux, L. Andric, M. Nakano, Y. Hikosaka, K. Ito, T. Marchenko and O. Travnikova, *et al.*, *Phys. Rev. A: At., Mol., Opt. Phys.*, 2016, **94**, 013416.
14 R. Feifel, J. Eland, S. Carniato, P. Selles, R. Püttner, D. Koulentianos, T. Marchenko, L. Journel, R. Guillemin and G. Goldsztejn, *et al.*, *Sci. Rep.*, 2017, **7**, 1–11.
15 D. Koulentianos, R. Püttner, G. Goldsztejn, T. Marchenko, O. Travnikova, L. Journel, R. Guillemin, D. Céolin, M. N. Piancastelli and M. Simon, *et al.*, *Phys. Chem. Chem. Phys.*, 2018, **20**, 2724–2730.
16 D. Koulentianos, S. Carniato, R. Püttner, G. Goldsztejn, T. Marchenko, O. Travnikova, L. Journel, R. Guillemin, D. Céolin and M. Rocco, *et al.*, *J. Chem. Phys.*, 2018, **149**, 134313.
17 T. Marchenko, S. Carniato, G. Goldsztejn, O. Travnikova, L. Journel, R. Guillemin, I. Ismail, D. Koulentianos, J. Martins and D. Céolin, *et al.*, *J. Phys. B: At., Mol. Opt. Phys.*, 2020, **53**, 224002.
18 N. Berrah, L. Fang, B. Murphy, T. Osipov, K. Ueda, E. Kukk, R. Feifel, P. van der Meulen, P. Salen and H. T. Schmidt, *et al.*, *Proc. Natl. Acad. Sci. U. S. A.*, 2011, **108**, 16912–16915.
19 P. Salén, P. van der Meulen, H. Schmidt, R. Thomas, M. Larsson, R. Feifel, M. N. Piancastelli, L. Fang, B. Murphy and T. Osipov, *et al.*, *Phys. Rev. Lett.*, 2012, **108**, 153003.
20 V. Zhaunerchyk, M. Kamińska, M. Mucke, R. Squibb, J. H. Eland, M. N. Piancastelli, L. Frasinski, J. Grilj, M. Koch and B. McFarland, *et al.*, *J. Phys. B: At., Mol. Opt. Phys.*, 2015, **48**, 244003.
21 M. Mucke, V. Zhaunerchyk, L. Frasinski, R. J. Squibb, M. Siano, J. H. Eland, P. Linusson, P. Salén, P. Vd Meulen and R. Thomas, *et al.*, *New J. Phys.*, 2015, **17**, 073002.
22 D. Koulentianos, A. Fouda, S. H. Southworth, J. D. Bozek, J. Küpper, R. Santra, N. Kryzhevoi, L. S. Cederbaum, C. Bostedt and M. Messerschmidt, *et al.*, *J. Phys. B: At., Mol. Opt. Phys.*, 2020, **53**, 244005.
23 L. Cederbaum, F. Tarantelli, A. Sgamellotti and J. Schirmer, *J. Chem. Phys.*, 1986, **85**, 6513–6523.
24 H. Ågren, J. Nordgren, L. Selander, C. Nordling and K. Siegbahn, *J. Electron Spectrosc. Relat. Phenom.*, 1978, **14**, 27–39.
25 K. Siegbahn, C. Nordling, A. Fahlman, R. Nordberg, K. Harmin, J. Hedman, G. Johansson, T. Bergmark, S. Karlsson and I. Lindgren, *et al.*, *Nova Acta Regiae Societatis Scientiarum Upsaliensis*, 1967, **20**, 282.
26 O. Takahashi, M. Tashiro, M. Ehara, K. Yamasaki and K. Ueda, *J. Phys. Chem. A*, 2011, **115**, 12070–12082.
27 R. Martin and D. Shirley, *J. Chem. Phys.*, 1976, **64**, 3685–3689.
28 T. Mazza, M. Ilchen, M. D. Kiselev, E. V. Gryzlova, T. M. Baumann, R. Boll, A. De Fanis, P. Grychtol, J. Montaño, V. Music, Y. Ovcharenko, N. Rennhack, D. E. Rivas, P. Schmidt, R. Wagner, P. Ziolkowski, N. Berrah, B. Erk, P. Johnsson, C. Küstner-Wetekam, L. Marder, M. Martins, C. Ott, S. Pathak, T. Pfeifer, D. Rolles, O. Zatsarinny, A. N. Grum-Grzhimailo and M. Meyer, *Phys. Rev. X*, 2020, **10**, 041056.
29 S. Carniato, *J. Electron Spectrosc. Relat. Phenom.*, 2020, **239**, 146931.
30 M. Štuhec, A. Kodre, M. Hribar, D. Glavič-Cindro, I. Arčon and W. Drube, *Phys. Rev. A: At., Mol., Opt. Phys.*, 1994, **49**, 3104.
31 C. Reynaud, M. Gaveau, P. Millié, S. Bodeur, P. Archirel, B. Lévy and I. Nenner, *J. Electron Spectrosc. Relat. Phenom.*, 1996, **79**, 357–360.
32 O. Travnikova, T. Marchenko, G. Goldsztejn, K. Jänkälä, N. Sisourat, S. Carniato, R. Guillemin, L. Journel, D. Céolin and R. Püttner, *et al.*, *Phys. Rev. Lett.*, 2016, **116**, 213001.
33 O. Travnikova, N. Sisourat, T. Marchenko, G. Goldsztejn, R. Guillemin, L. Journel, D. Céolin, I. Ismail, A. Lago and R. Püttner, *et al.*, *Phys. Rev. Lett.*, 2017, **118**, 213001.
34 R. Püttner, I. Dominguez, T. Morgan, C. Cisneros, R. Fink, E. Rotenberg, T. Warwick, M. Domke, G. Kaindl and A. Schlachter, *Phys. Rev. A: At., Mol., Opt. Phys.*, 1999, **59**, 3415.
35 N. Kosugi, E. Shigemasa and A. Yagishita, *Chem. Phys. Lett.*, 1992, **190**, 481–488.
36 R. Feifel, Y. Velkov, V. Carravetta, C. Angeli, R. Cimiraglia, P. Sałek, F. Gel'mukhanov, S. Sorensen, M. Piancaśtelli and A. De Fanis, *et al.*, *J. Chem. Phys.*, 2008, **128**, 064304.
37 R. Püttner and K. Ueda, *J. Chem. Phys.*, 2016, **145**, 224302.
38 J.-P. Rueff, J. Ablett, D. Céolin, D. Prieur, T. Moreno, V. Balédent, B. Lassalle-Kaiser, J. Rault, M. Simon and A. Shukla, *J. Synchrotron Radiat.*, 2015, **22**, 175–179.
39 D. Céolin, J. Ablett, D. Prieur, T. Moreno, J.-P. Rueff, T. Marchenko, L. Journel, R. Guillemin, B. Pilette and T. Marin, *et al.*, *J. Electron Spectrosc. Relat. Phenom.*, 2013, **190**, 188–192.
40 L. Werme, T. Bergmark and K. Siegbahn, *Phys. Scr.*, 1973, **8**, 149.
41 G. King, M. Tronc, F. Read and R. Bradford, *J. Phys. B: At. Mol. Phys.*, 1977, **10**, 2479.
42 T. H. Dunning Jr, *J. Chem. Phys.*, 1989, **90**, 1007–1023.
43 A. Szabo and N. S. Ostlund, *Modern quantum chemistry: introduction to advanced electronic structure theory*, Courier Corporation, 2012.
44 W. Hunt, T. Dunning Jr and W. Goddard III, *Chem. Phys. Lett.*, 1969, **3**, 606–610.
45 H. Ågren, V. Carravetta, L. G. Pettersson and O. Vahtras, *Phys. B*, 1995, **208**, 477–480.
46 O. Plashkevych, L. Yang, O. Vahtras, H. Ågren and L. G. Petterson, *Chem. Phys.*, 1997, **222**, 125–137.
47 O. Plashkevych, V. Carravetta, O. Vahtras and H. Ågren, *Chem. Phys.*, 1998, **232**, 49–62.
48 V. Carravetta, O. Plashkevych and H. Ågren, *J. Chem. Phys.*, 1998, **109**, 1456–1464.
49 V. Carravetta, O. Plashkevych and H. Ågren, *Chem. Phys.*, 2001, **263**, 231–242.
50 B. J. Dalton, *Theory and applications of moment methods in many-fermion systems*, Springer Science & Business Media, 2012.

51 E. Clementi, *Modern techniques in computational chemistry: MOTECC-91*, Springer Science & Business Media, 1991, vol. 91.
52 NIST Chemistry WebBook, NIST Standard Reference Database Number 69.
53 M. W. Schmidt, K. K. Baldridge, J. A. Boatz, S. T. Elbert, M. S. Gordon, J. H. Jensen, S. Koseki, N. Matsunaga, K. A. Nguyen and S. Su, *et al.*, *J. Comput. Chem.*, 1993, **14**, 1347–1363.
54 A. D. Becke, *J. Chem. Phys.*, 1993, **98**, 5648–5652.
55 C. Lee, W. Yang and R. G. Parr, *Phys. Rev. B: Condens. Matter Mater. Phys.*, 1988, **37**, 785.
56 T. Sham, B. Yang, J. Kirz and J. Tse, *Phys. Rev. A: At., Mol., Opt. Phys.*, 1989, **40**, 652.
57 A.-P. Hitchcock and C. Brion, *J. Electron Spectrosc. Relat. Phenom.*, 1980, **18**, 1–21.
58 K. R. Seddon, Gmelin handbook of inorganic chemistry, Fluorine, Supplement Volume 4: Compounds with Oxygen and Nitrogen: Springer-Verlag, Berlin, Heidelberg, New York, Tokyo, 1986, xviii+ 409 pages, DM 1684. ISBN3-540-93536-3, 1987.
59 G. Frenking, W. Koch, D. Cremer, J. Gauss and J. F. Liebman, *J. Phys. Chem.*, 1989, **93**, 3410–3418.
60 G. Herzberg and J. W. T. Spinks, *Molecular Spectra and Molecular Structure. I. Spectra of Diatomic Molecules… [Translated by John WT Spinks.]*, D. Van Nostrand Company, 1950.
61 R. Püttner, T. Arion, M. Förstel, T. Lischke, M. Mucke, V. Sekushin, G. Kaindl, A. Bradshaw and U. Hergenhahn, *Phys. Rev. A: At., Mol., Opt. Phys.*, 2011, **83**, 043404.
62 M. Žitnik, R. Püttner, G. Goldsztejn, K. Bučar, M. Kavčič, A. Mihelič, T. Marchenko, R. Guillemin, L. Journel and O. Travnikova, *et al.*, *Phys. Rev. A*, 2016, **93**, 021401.
63 C. Nicolas and C. Miron, *J. Electron Spectrosc. Relat. Phenom.*, 2012, **185**, 267–272.
64 M. Piancastelli, D. Lindle, T. Ferrett and D. Shirley, *J. Chem. Phys.*, 1987, **86**, 2765–2771.
65 M. Piancastelli, *J. Electron Spectrosc. Relat. Phenom.*, 1999, **100**, 167–190.
66 M. A. Vincent and I. H. Hillier, *J. Chem. Soc., Faraday Trans. 2*, 1988, **84**, 1229–1236.
67 R. C. Couto, L. Kjellsson, H. Ågren, V. Carravetta, S. L. Sorensen, M. Kubin, C. Bülow, M. Timm, V. Zamudio-Bayer and B. von Issendorff, *et al.*, *Phys. Chem. Chem. Phys.*, 2020, **22**, 16215–16223.
68 J. Stöhr, *NEXAFS spectroscopy*, Springer Science & Business Media, 2013, vol. 25.
69 M. Domke, C. Xue, A. Puschmann, T. Mandel, E. Hudson, D. Shirley and G. Kaindl, *Chem. Phys. Lett.*, 1990, **173**, 122–128.
70 S. Oberli, N. Sisourat, P. Selles and S. Carniato, *Phys. Rev. A*, 2018, **97**, 013406.

